Journal of Magnetism and Magnetic Materials 115 (1992) 197–203
North-Holland

journal of magnetism and magnetic materials

The complex permeability and harmonic generation of a $Bi_2Sr_2CaCu_2O_{8-y}$ crystal: measurements and models

Q.H. Lam [1], C.D. Jeffries, A. Behrooz, G. Briceno and A. Zettl

Department of Physics, University of California at Berkeley, and Materials Science Division, Lawrence Berkeley Laboratory, Berkeley, CA 94720, USA

Received 20 November 1991; in revised form 17 February 1992

For a single crystal of $Bi_2Sr_2CaCu_2O_{8-y}$ at 77 K and subject to simultaneous ac and dc magnetic fields, measurements are reported for the complex ac permeability ($\mu' - i\mu''$) and for the generated harmonic power $P(nf)$. A plot of μ'' versus $\log_{10}(H_{ac})$ shows one peak at $H_{ac} = 5.2$ Oe, which is interpreted as the penetration field H^* in a critical state model. This result corresponds to only one component of the supercurrent, in contrast to both inter- and intragranular components generally observed in $YBa_2Cu_3O_{7-\delta}$. The observed dependence of μ', μ'' and $P(nf)$ on H_{dc} and H_{ac} are only moderately well explained by a generalized critical state model.

1. Introduction

High-temperature superconductors have a complex microstructure; both inter- and intragranular supercurrents have been identified in polycrystalline $YBa_2Cu_3O_{7-\delta}$ (YBCO) (see, for example, refs. [1–4]). Contactless measurements of the ac permeability $\tilde{\mu} = \mu' - i\mu''$ and generation of harmonic power $P(nf)$ in applied ac and dc magnetic fields, together with detailed interpretation by critical state models, have provided much information on critical current densities [4–7]. Data on harmonic generation in a single crystal of YBCO, first reported by Xenikos and Lemberger [8], were explicable by a simple dynamical model based on flux creep resistance.

In this paper we extend such previous measurements to a single crystal of $Bi_2Sr_2CaCu_2O_{8-y}$ (BSCCO) at 77 K. Only one component of the supercurrent is observed, implying that there is no significant contribution to $\tilde{\mu}$ from weak links. We find *modest* agreement between the overall data and critical state models, in contrast to YBCO thin films and ceramic rods, where unusually detailed agreement is found.

2. Experimental procedures

The $Bi_2Sr_2CaCu_2O_{8-y}$ single crystal was grown from a mixture of Bi_2O_3, CuO, $SrCO_3$ and $CaCO_3$ with molar percentage of 22.4%, 32%, 26.9% and 18.7%, respectively. More details of the growth procedure have been described elsewhere [9]. The crystal is roughly disk-shaped with a radial dimension $R \approx 1.5$ mm and thickness $d \approx 0.01$ mm, with the c-axis perpendicular to the disk plane. The transition temperature is found to be $T_c = 88$ K, from four-probe dc resistance and dc magnetic susceptibility measurements; the full resistive transition width is of order 2.5 K.

The apparatus to measure $\tilde{\mu}$ and $P(nf)$ consists of coaxial copper coils, cooled in liquid N_2 in

Correspondence to: Prof. C.D. Jeffries, Department of Physics, Room 366, LeConte Hall, University of California at Berkeley, Berkeley, CA 94720, USA. Tel.: +1-510-642-3382; telefax: +1-510-643-8497.

[1] Present address: IBM Almaden Research Center, 650 Harry Road, San Jose, CA 95120, USA.

a magnetically shielded dewar. These coils are driven by highly stable synthesizers to produce a magnetic field

$$H_a(t) = H_{dc} + H_1 \cos(\omega t), \tag{1}$$

oriented along the c-axis of the crystal, which is mounted in a coaxial "signal" coil of $N = 324$ turns and area $A = 0.95$ cm^2. An identical coil, counterwound and empty, is used with a simple balancing circuit to null out the direct pickup signal $\sim dH_a(t)/dt$. The resulting signal voltage $V(t)$ is proportional to the time-derivative of the sample ac magnetization and has the form $V(t) = \sum_{n=1}^{\infty} V_n(t) = \sum_{n-1}^{\infty} [V_n' \sin(n\omega t) + V_n'' \cos(n\omega t)]$. The harmonic components are due to the nonlinearity of the electrodynamical behavior of the material. For $n = 1$ the sine and cosine signal components $V_1' \propto \mu_1' H_1$ and $V_1'' \propto \mu_1'' H_1$ are separately measured by a lock-in detector. For $n = 2,3,\ldots,20$, the power spectrum $P(nf) \propto [(V_n')^2 + V_n'')^2]$ is recorded by an analog spectrum analyzer (HP 3585A).

3. Critical state model

In 1962 Bean [10] introduced the idea of a critical state in type-II superconductors which successfully explained flux trapping and hysteresis in dc magnetization measurements observed in conventional low-temperature superconductors. The idea was extended by Anderson and Kim [11] who introduced a parameter α representing the fluxon pinning force density arising from lattice defects and impurities in the superconductor. More recently the model has been further extended in various ways for the investigation of the electrodynamics of high-temperature superconductors in applied ac and dc magnetic fields [4–7]. We briefly review here a *generalized* critical state model which has been used successfully for YBCO [4,5].

For simplicity, we first ignore the demagnetization effects for the thin crystal and consider a homogeneous sample with the geometry of a long cylinder with radius R; the demagnetization effects of a disk-shaped geometry will be discussed later. The magnetic field $H_a(t) = H(r = R, t)$ is applied parallel to the axis of the sample. For $H_a > H_{c1}$, where H_{c1} is the lower critical field of the material, it is energetically favorable for vortices to enter the sample, resulting in an internal magnetic field profile $H(r)$. The field penetrates the sample to a depth dependent on the critical current density J_c of the sample, which we assume to have the general form (Gaussian units)

$$J_c(H) = \frac{\alpha' c}{(|H| + H_0)^{\beta}}, \tag{2}$$

where α', H_0, and β are parameters to be determined by the data. Here $\alpha(H) \equiv \mu_{eff}\alpha'/(|H| + H_0)^{\beta-1}$ is the vortex pinning force density introduced by Anderson and Kim [11,12], and β is a parameter controlling the field dependence of J_c. The Bean model assumes $\beta = 0$; the Anderson–Kim model assumes $\beta = 1$. We will determine β experimentally. The critical state model assumes that the sample's local shielding current density J would be either zero in regions which have not yet been exposed to magnetic flux, or $J_c(H)$ in regions which have been subjected to an electromotive force induced by the motion of flux vortices. This assumption, together with Ampere's law, leads to the following critical state equation for cylindrical geometry:

$$\frac{dH}{dr} = \pm \frac{4\pi}{c} J_c(H). \tag{3}$$

The sign in eq. (3) is determined by whether the supercurrent is trying to screen out entering magnetic flux lines or, if the applied magnetic field is being decreased, to confine the flux lines that have already entered the sample. Eqs. (1), (2) and (3) are solved analytically to find $H(r, H_a(t))$, where $0 < r < R$, $0 < t < 2\pi/\omega$. From this we derive an analytical expression for the spatial average induction field in the sample:

$$\langle B(t) \rangle \equiv (\mu_{eff}/\pi R^2) \int_0^R H(r, t) 2\pi r \, dr, \tag{4}$$

and its time-derivative $d\langle B(t)\rangle/dt$. From a discrete time series ($N = 2048$) of $d\langle B(t))\rangle/dt$ a fast Fourier transform is used to compute the ac

permeability components μ_1', μ_1'' and the harmonic power $P(nf)$ of the sample, as a function of the experimentally known parameters (H_{dc}, H_1, R) and of those to be fit by the data (α', H_0, β). However, the model further yields a relationship

$$H^* = \left[H_0^{\beta+1} + 4\pi(\beta+1)\alpha' R\right]^{1/(\beta+1)} - H_0, \tag{5}$$

where H^* is the value of the applied field H_a at which the penetrated flux front just reaches $r = 0$; for $H_{dc} = 0$ this corresponds to a peak of $\mu_1''(H_1)$ at $H_1 = H^*$ which can be readily measured experimentally, leaving only two independent parameters, β and H_0, to be fit by the overall experimental data.

4. Results and discussion

All the following data on the $Bi_2Sr_2CaCu_2O_{8-y}$ single crystal are taken at 77 K with both the ac and dc magnetic fields perpendicular to the a–b plane of the crystal.

In fig. 1, the circles are experimental data of the inductive and dissipative components of the complex permeability, μ_1' and μ_1'', taken on this single crystal, measured over four decades of the ac magnetic field amplitude H_1, from ~ 0.1 to 600 Oe, at 85 Hz. Only one peak in the dissipative component μ_1'' is observed (in contrast with the two peaks observed in bulk ceramic $YBa_2Cu_3O_{7-\delta}$ [4], representing separate contributions from inter- and intragranular components of supercurrents). The value of the μ_1'' peak position, H^*, is quite small: $H^* = 5.2$ Oe. This μ_1'' peak is located at the same position as the inflection point of μ_1'. Because μ_1' approaches a plateau at value 1 for $H_1 \gg H^*$, full flux penetration of the sample is achieved by the maximum ac field available from our apparatus, and therefore no more dissipation peaks are expected beyond $H_1 > 600$ Oe. We were unable to detect any peak below $H_1 = 0.1$ Oe, limited by the signal-to-noise ratio of the apparatus. Thus, this μ_1'' peak at $H^* = 5.2$ Oe is ascribed to the "one and only intrinsic" supercurrent of the single crystal sample.

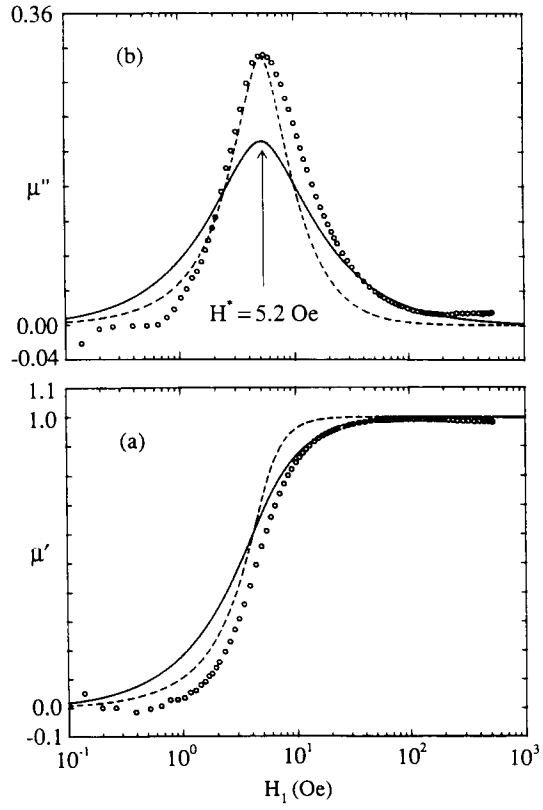

Fig. 1. Open circles: experimental measurements (Gaussian units) of (a) μ_1'' and (b) μ_1' versus $\log_{10}(H_1)$ for $Bi_2Sr_2CaCu_2O_{8-y}$ single crystal, $H_{dc} = 0$, $T = 77$ K, $f = 85$ Hz. Dashed lines: generalized critical state model calculations with $\beta = 1.3$, $H_0 = 3$ Oe and $H^* = 5.2$ Oe. Solid lines: Bean model calculations (i.e. $\beta = 0$) with $H^* = 5.2$ Oe.

In order to use the critical state model to fit the experimental data and to deduce J_c using eqs. (2), (3) and (5), the significant demagnetization effects of the disk-shaped single crystal sample have to be addressed. Daeumling and Larbalestier [13] treated this demagnetization problem for the critical state in disk-shaped superconductors in the special case that J_c is assumed to be independent of the magnetic field. They divided the disk into ring segments, and calculated self-consistently the current distributions and magnetic field vectors due to the combined contributions of the ring-segment currents in addi-

tion to the applied magnetic field. They found that the field shielded (or trapped) in the center of the disk, which they denoted by h^*, was approximately $h^* = (\pi/c)J_c d$, where d is the *thickness* of the disk. Note that in the absence of demagnetization, one would calculate, from eq. (3) and Bean's assumption that J_c is independent of H (i.e. $\beta = 0$ in eq. (2)), that $H^* = (4\pi/c)J_c R$, where R is the *radius* of the disk. The shielding currents also create radial fields which are of order $(2\pi/c)J_c d$ on the disk surface. For low applied fields $H_a < h^*$ these self-field effects dominate, leading to substantial deviation of the local field from the applied field. They also find that the demagnetization field does not depend on the applied field, but rather on J_c. So if $H_a \gg h^*$, a demagnetization correction is then not necessary. In short, the surprisingly simple result of ref. [13] seems to indicate that the sample radius R should be replaced by the thickness d in the calculation of the critical current for a thin sample.

Another theoretical study of the ac susceptibility of thin superconducting films near T_c has been given by Sun et al. [14], who point out the difficulties of this intrinsically nonlinear problem.

We use Daeumling and Larbalestier's results, notwithstanding their special case of J_c being assumed constant, to get an estimate of J_c of this single crystal as $J_c = cH^*/4\pi d \approx 4.1 \times 10^3$ A/cm^2, where the thickness of the crystal is $d \approx 10$ μm. This estimated value should correspond to some averaged value of J_c over the sample, which in turn is approximately equal to $J_c(H \approx H^*/2 = 2.6$ Oe) [4]. This small value of J_c is most likely due to a small flux pinning force density in the sample. The dashed lines in fig. 1 are calculations according to the generalized critical state model, eqs. (2), (3) and (5), using the best fitting values $\beta = 1.3$ and $H_0 = 3$ Oe, and the measured value $H^* = 5.2$ Oe. The calculated μ_1'' peak has the same amplitude as the experimental data. These calculations have been done by simple-mindedly using the generalized critical state model for cylindrical geometry, but replacing the lateral dimension of the sample by the thickness, "R" $\rightarrow d = 10$ μm. Calculations according to the special case of the Bean version

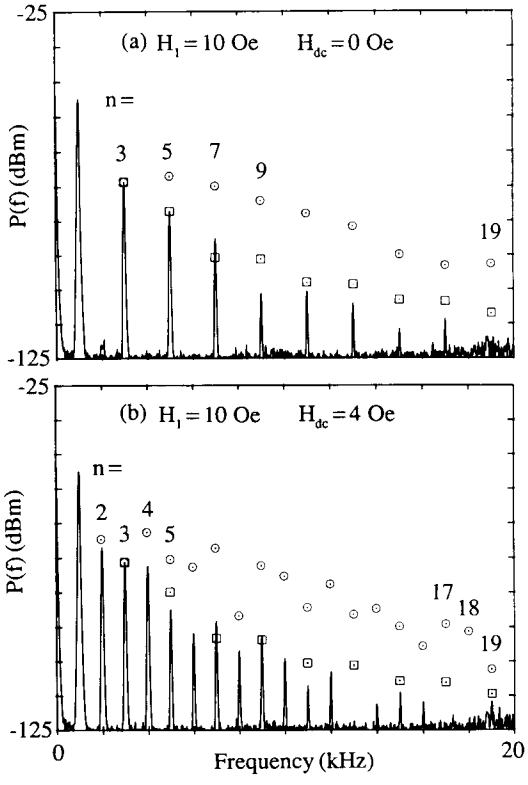

Fig. 2. (a) Harmonic spectra generated by $Bi_2Sr_2CaCu_2O_{8-y}$ single crystal taken at $T = 77$ K, $f = 1.0$ kHz and ac field amplitude $H_1 = 10.0$ Oe. The values of the dc magnetic field H_{dc} are (a) 0.0 and (b) 4.0 Oe. The circles are the harmonic spectra predicted by the generalized critical state model calculations with $\beta = 1.3$, $H_0 = 3$ Oe and $H^* = 5.2$ Oe. The squares are the $\beta = 0$ model calculations with $H^* = 5.2$ Oe. Note that for the $\beta = 0$ model, in which J_c is independent of the magnetic field, no even harmonics should be generated even when $H_{dc} \neq 0$.

critical state model [15], i.e. with $\beta = 0$, are also plotted for comparison in fig. 1, as solid lines. The generalized critical state model fits the data better for $H_1 \leq H^*$ and the amplitude of the peak; whereas the $\beta = 0$ model seems to fit better for $H_1 > H^*$, but it fails to fit the amplitude.

The measured harmonic power spectrum, $P(nf)$ versus n, of the signal voltage for $H_1 = 10$ Oe, $H_{dc} = 0$, $f = \omega/2\pi = 1.0$ kHz is shown as a solid line in fig. 2a; the dot-circles represent the calculated harmonic spectra according to the generalized critical state model, using the parameter set, $\beta = 1.3$, $H_0 = 3$ Oe and $H^* = 5.2$ Oe, men-

tioned previously, while the dot-squares represent the $\beta = 0$ model calculation results. Although the generalized critical state model calculations give a satisfactory fit for μ_1' and μ_1'' versus $\log_{10}(H_1)$ in fig. 1, it predicts stronger harmonic power generation than actually observed. In contrast, the $\beta = 0$ model calculations seem to fit the power spectra better in fig. 2a. Fig. 2b shows power spectra for $H_1 = 10$ Oe and $H_{dc} = 4$ Oe; the data show both even and odd harmonics. However, the $\beta = 0$ model predicts *zero intensity* for even harmonics, even in the presence of a dc magnetic field. Thus we must reject the value $\beta = 0$ on the basis of symmetry. Since any model with $\beta > 0$ predicts nonzero even harmonics through symmetry breaking, parameter sets with a small value of β have also been tried to fit the data. Although for, say, $\beta = 0.1$, model calculations explain the even harmonics, they consistently failed to fit the μ_1' and μ_1'' versus $\log_{10}(H_1)$ data in fig. 1, for all $\beta \leq 0.5$. The circles in fig. 2b are predictions by the same parameter set as in fig. 1 and fig. 2a; even harmonics are predicted, but they do not fit the overall data very well.

In fig. 3, for $H_{dc} = 0$, $f = 1.0$ kHz, odd harmonic powers taken experimentally as a function of $\log_{10}(H_1)$ are shown as circles for harmonic numbers $n = 3, 5, 7, 9$. The dashed lines are the generalized critical state model calculations with $\beta = 1.3$, $H_0 = 3$ Oe and $H^* = 5.2$ Oe, whereas the solid lines are the corresponding $\beta = 0$ model calculations. The critical state model calculations give approximately the observed slopes for $H_1 < 10$ Oe. In fig. 3a for the 3rd harmonic power, $P(3f) \sim H^{4.7}$ [6]. Neither model fits the details of the harmonic power versus ac field amplitude data satisfactorily, especially for $H_1 > 10$ Oe. In particular, the dips in $P(nf)$ in figs. 3b–d do not correspond to any model predicted dips.

The effects of adding a dc field $H_{dc} = 10.2$ Oe on the 7th harmonic power are shown in fig. 4, which is typical of other harmonics. The data (circles) are in fair agreement with the generalized model (dashed line) previously described;

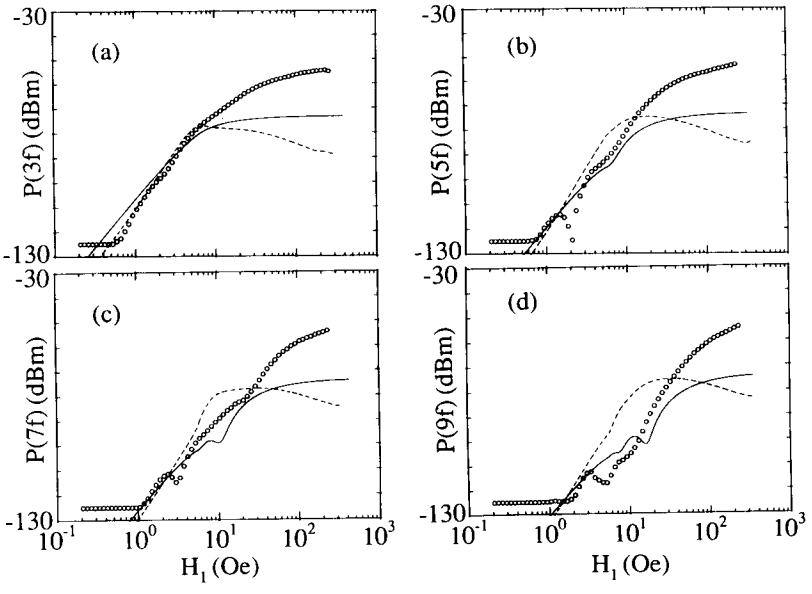

Fig. 3. (a) Circles: third harmonic power (10 dB/div) versus $\log_{10}(H_1)$ experimentally measured on $Bi_2Sr_2CaCu_2O_{8-y}$ single crystal at $T = 77$ K, $f = 1.0$ kHz, $H_{dc} = 0$. Dashed line: generalized critical state model calculations with $\beta = 1.3$, $H_0 = 3$ Oe and $H^* = 5.2$ Oe. Solid line: Bean model predictions with $H^* = 5.2$ Oe. (b–d) Same measurements and calculations for the 5th, 7th and 9th harmonics.

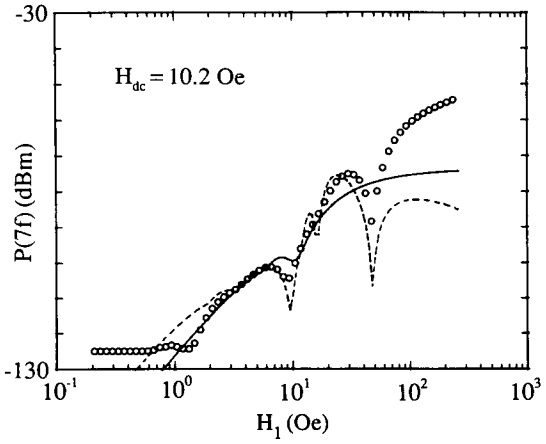

Fig. 4. Circles: 7th harmonic power (10 dB/div) versus $\log_{10}(H_1)$ experimentally measured on BSCCO single crystal with $H_{dc} = 10.2$ Oe, $T = 77$ K, $f = 1.0$ kHz. Dashed line: generalized critical state model calculations with $\beta = 1.3$, $H_0 = 3$ Oe and $H^* = 5.2$ Oe. Solid line: $\beta = 0$ model predictions with $H^* = 5.2$ Oe.

other parameter sets predict dip positions which do not match the data. The $\beta = 0$ model (solid line) is also plotted for comparison. We note that in a YBCO ceramic rod such $P(nf)$ versus H_1 data can be very well fit by a generalized critical state model [16].

Additional measurements, at $f = 1$ kHz, not shown here, on $P(nf)$ versus H_{dc} for $n = 2, \ldots, 20$ show: for even harmonics, dips at $H_{dc} = 0$; for odd harmonics, peaks at $H_{dc} = 0$; and a series of dips spaced very roughly by $\Delta H \approx 3H_1/n$. The generalized critical state model with parameters used in fig. 3 predicts very uniformly spaced peaks. The $\beta = 0$ model predicts $P(nf) = 0$ for n even and $P(nf) =$ constant for n odd, even less satisfactorily than the generalized critical state model.

5. Summary and conclusions

We have reported new experimental results at 77 K for a thin crystal of Bi–Sr–Ca–Cu–O for the complex permeability $\tilde{\mu}_1$ and generated harmonic power $P(nf)$ as a function of H_{dc} and H_{ac}, and have attempted to fit it with a generalized critical state model. In fig. 1 only one peak in μ_1'' is found at $H_1 = 5.2$ Oe in the measurement range 0.1 Oe $< H_1 <$ 600 Oe, with a corresponding inflection in μ_1'; this single μ_1'' peak corresponds to only one component of the supercurrent, presumably intrinsic. A qualitative prediction of μ_1' and μ_1'' versus H_1 is obtained by the generalized critical state model. The Bean model, with $\beta = 0$, fails to explain the observed even harmonics in the presence of a dc field, fig. 2b, and can be ruled out. We note that in experiments in which $H_{dc} = 0$ (fig. 1, fig. 2a, and fig. 3), it is not as easy to rule out $\beta = 0$; this indicates the advantage of using harmonic analysis to detect any symmetry breaking upon application of a dc field. Assuming that the μ_1'' peak corresponds to the penetration field H^* in a critical state model, we can, using thin sample correction calculations as described by Daeumling and Labalestier, find an approximate critical current density in zero dc field, $J_c \approx 4 \times 10^3$ A/cm^2 at 77 K. However, we note that this calculated value is approximately equal to $J_c(H)$ at $H \approx H^*/2 = 2.6$ Oe.

Our overall conclusion is that the modified critical state model, together with our simplified approximations for the thin sample using the results of Daeumling and Labalestier, does not quantitatively explain our data for the BSCCO crystal. A more exact numerical solution to the problem is beyond the scope of this paper. Finally, we note that the models of Xenikos and Lemberger [8], and of Sun et al. [14], may be viable alternatives.

Acknowledgement

This work was supported in part by the Director, Office of Energy Research, Office of Basic Energy Sciences, and Materials Sciences Division of the U.S. Department of Energy under Contract No. DE-AC03-76SF00098.

References

[1] D. Dimos, P. Chaudhari and J. Mannhart, Phys. Rev. B 41 (1990) 4038.

[2] R.B. Goldfarb, A.F. Clark, A.I. Braginski and A.J. Panson, Cryogenics 27 (1987) 475.
[3] B. Renker, I. Apfelstedt, H. Küpfer, C. Politis, H. Rietschel, W. Schauer, H. Wühl, U. Gottwick, H. Kneissel, U. Rauchschwalbe, H. Spille and F. Steglich, Z. Phys. B 67 (1987) 1.
[4] Q.H. Lam, Y. Kim and C.D. Jeffries, Phys. Rev. B 42 (1990) 4846.
[5] Y. Kim, Q.H. Lam and C.D. Jeffries, Phys. Rev. B 43 (1991) 11404.
[6] L. Ji, R.H. Sohn, G.C. Spalding, C.J. Lobb and M. Tinkham, Phys. Rev. B 40 (1989) 10936.
[7] K.H. Müller, J.C. Macfarlane and R. Driver, Physica C 158 (1989) 366.
[8] D.G. Xenikos and T.R. Lemberger, Phys. Rev. B 41 (1990) 869.
[9] J.-M. Imer, F. Patthey, B. Dardel, W.-D. Schneider, Y. Baer, Y. Petroff and A. Zettl, Phys. Rev. Lett. 62 (1989) 336.
[10] C.P. Bean, Phys. Rev. Lett. 8 (1962) 250.
[11] P.W. Anderson and Y.B. Kim, Rev. Mod. Phys. 36 (1964) 39.
[12] P.W. Anderson, Phys. Rev. Lett. 9 (1962) 309.
[13] M. Daeumling and D.C. Larbalestier, Phys. Rev. B 40 (1989) 9350.
[14] J.Z. Sun, M.J. Scharen, L.C. Bourne and J.R. Schrieffer, Phys. Rev. B 44 (1991) 5275.
[15] C.P. Bean, Rev. Mod. Phys. 36 (1964) 31.
[16] Q.H. Lam and C.D. Jeffries, Physica C 194 (1992) 37.